Supporting Information

Strong yet tough bio-based biomimetic-multiphase composite polyesters with superior barrier and chemically closed-loop performance

Hao Wang[1, 2], Jiheng Ding[2,*], Qinchao Chu[1, 2], Hongran Zhao[2], Jin Zhu[2], Jinggang Wang[2, *]

[1]School of Materials Science and Chemical Engineering, Ningbo University, Ningbo, Zhejiang, 315211, China;

[2] Key Laboratory of Bio-based Polymeric Materials Technology and Application of Zhejiang Province, Ningbo Institute of Materials Technology and Engineering, Chinese Academy of Sciences, Ningbo 315201, China.

**Corresponding Authors:*

dingjh@nimte.ac.cn (Jiheng Ding),

wangjg@nimte.ac.cn (Jinggang Wang).

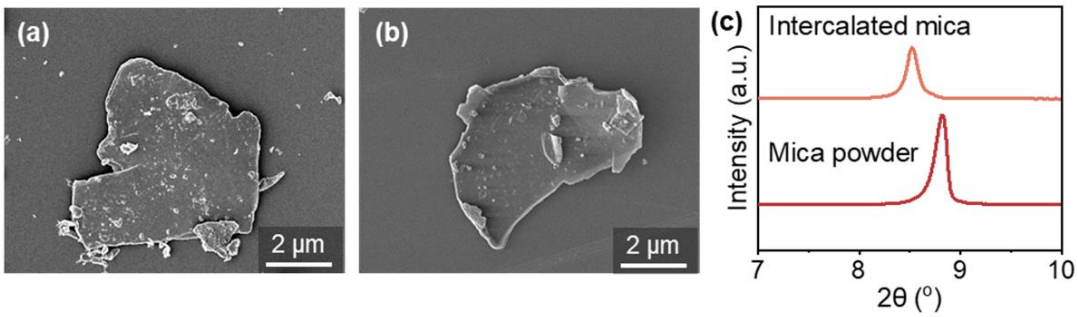

Figure S1. SEM images of bulk mica (a) and intercalated mica (b). XRD patterns of mica and intercalated mica (c). Typically, the bulk mica shows compact large block structure. After intercalation by ILs, the thickness of mica became thinner. It can be seen from the XRD results, after intercalation, the layer spacing of mica became larger.

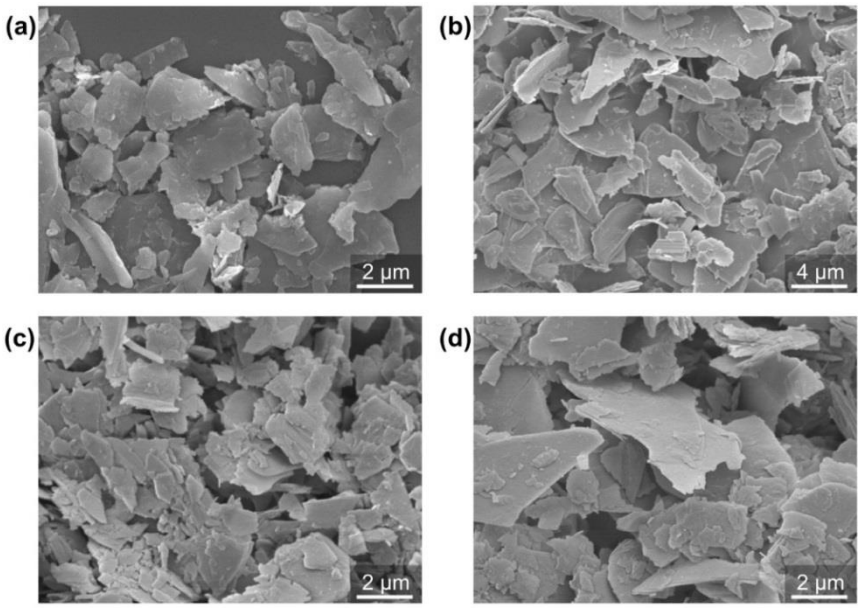

Figure S2. SEM images of MSSs through ILs assisted sonication exfoliation. Results demonstrate that the obtained MSSs have uniform size distribution and ultrathin feature.

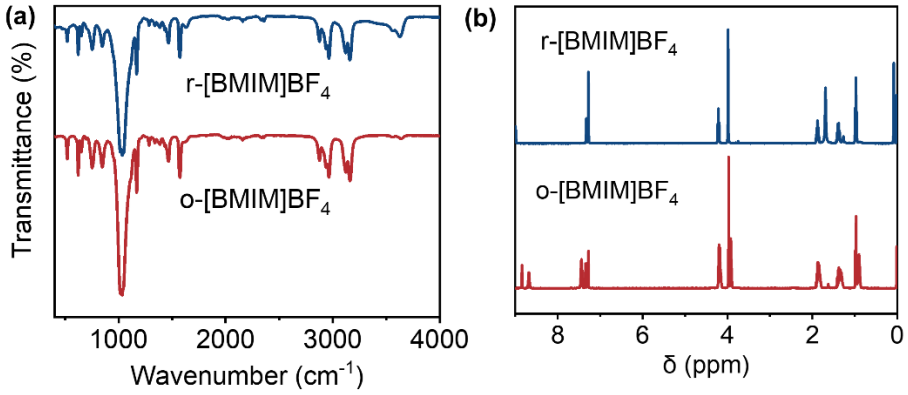

Figure S3. FTIR (a) and ^{1}H NMR (b) spectra of recycled ILs r-[BMIM]BF_4 and compared with the original ILs o-[BMIM]BF_4[1]. It can be observed that the chemical composition of r-[BMIM]BF_4 has not changed and it can continue to be utilized for mica exfoliation.

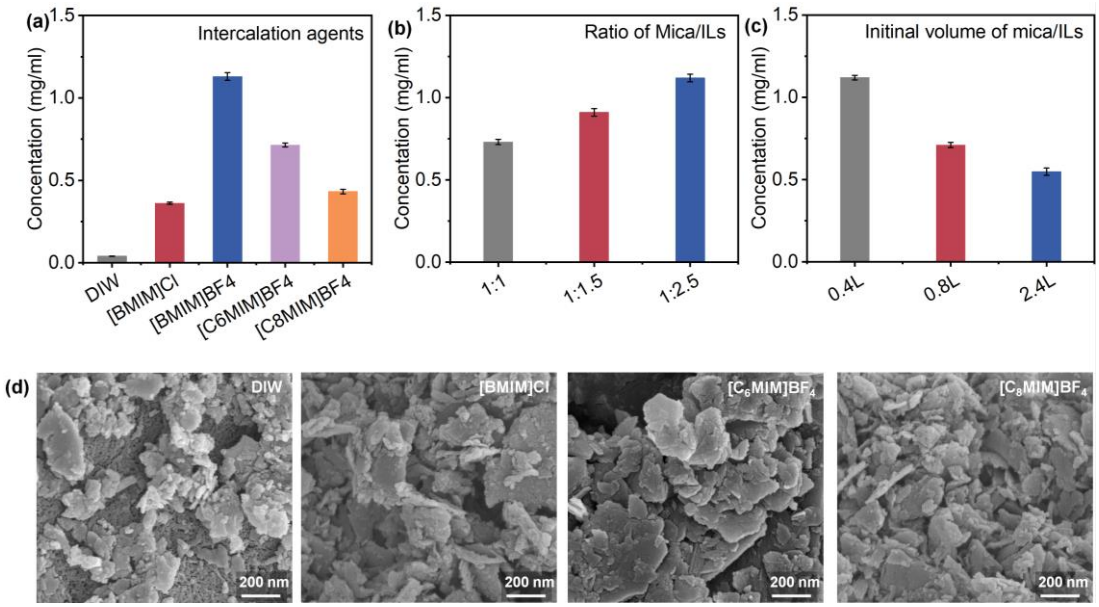

Figure S4. Different ILs (a), mass ratios (b), and liquid volumes (c) were used to exfoliate mica. The concentration of MSSs was calculated to screen for the optimal intercalation agent and stripping conditions. By comparing the concentration of MSSs and the SEM images (d) of MSSs, it was found that $[BMIM]BF_4$ is the optimal intercalation agent and the optimal exfoliation condition is when the ratio of ionic liquid to mica is 1:2.5.

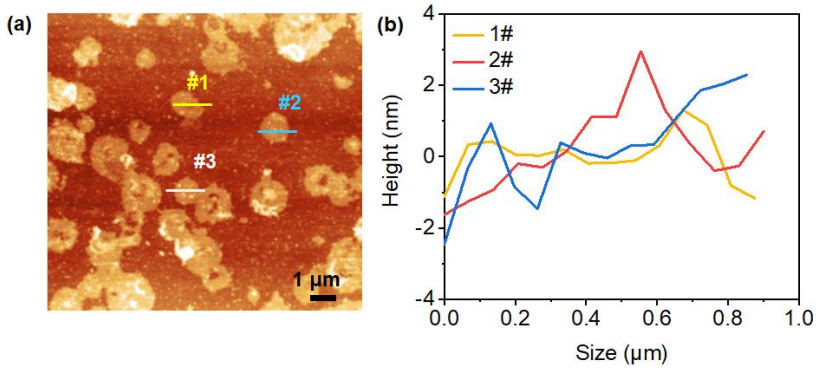

Figure S5. AFM image (a) and the corresponding height profiles (b) of the exfoliated MSSs. AFM results reveal that the MSSs with a thickness of 1.5 nm, indicating their single-layer feature.

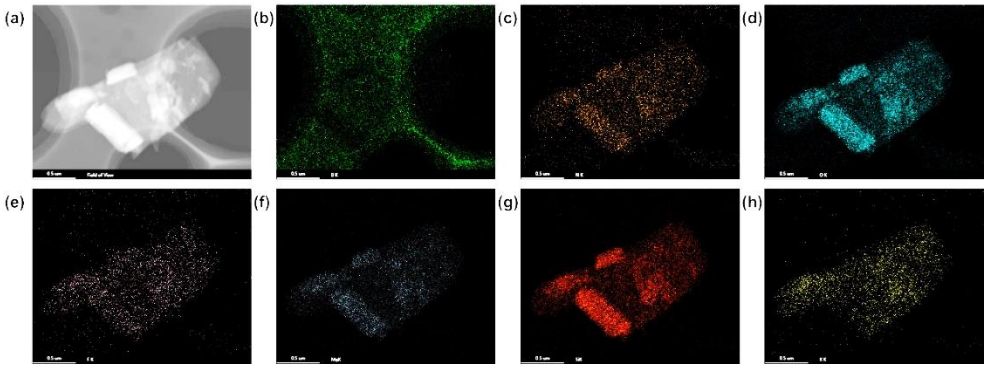

Figure S6. EDS images of MSSs through SEM testing (a). The element distribution mapping of (b) B atom, (c) N atom, (d) O atom, (e) F atom, (f) Mg atom, (g) Si atom, and (h) K atom. The elements are uniform distribution in the MSSs.

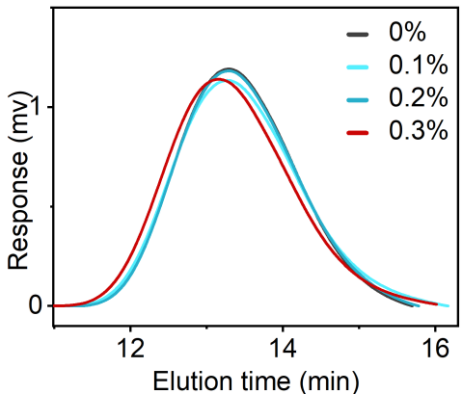

Figure S7. GPC chromatogram of PBF and BCP with different content of MSSs. The result shows that the addition of MSSs in PBF cannot change the molecular weight.

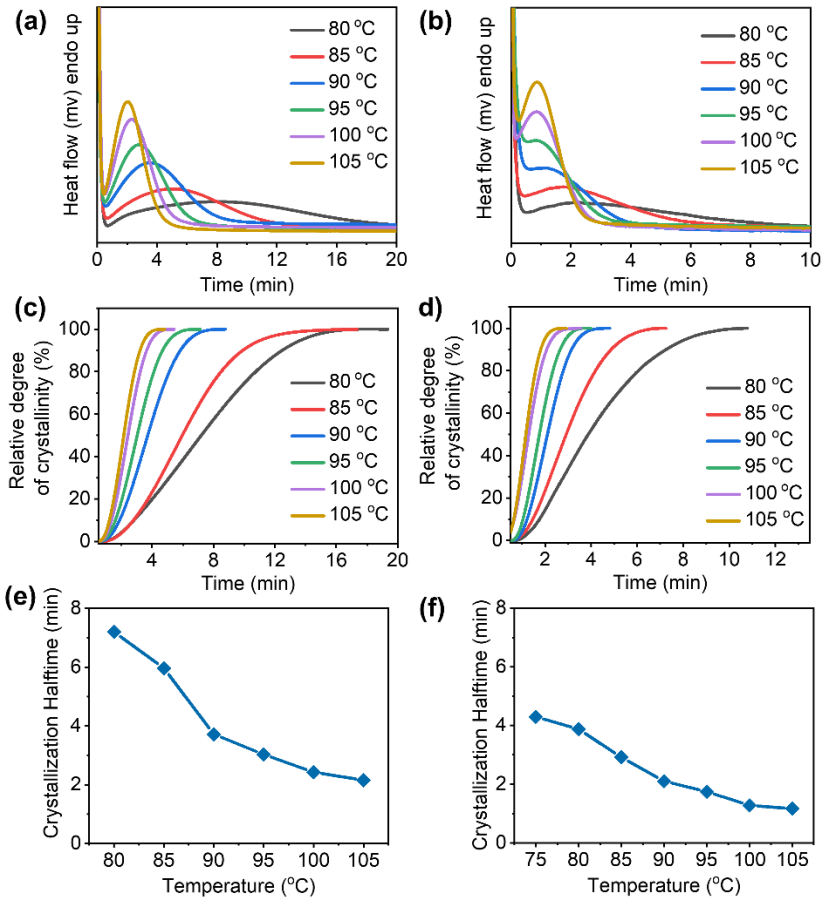

Figure S8. Isothermal crystallization peaks recorded at the indicated temperatures for PBF and BCP3 (a and b), Evolution of the relative degree of crystallinity with time for PBF and BCP3 (c and d). Halftime of crystallization versus the isothermal crystallization temperature for PBF and BCP3 (e and f) [2].

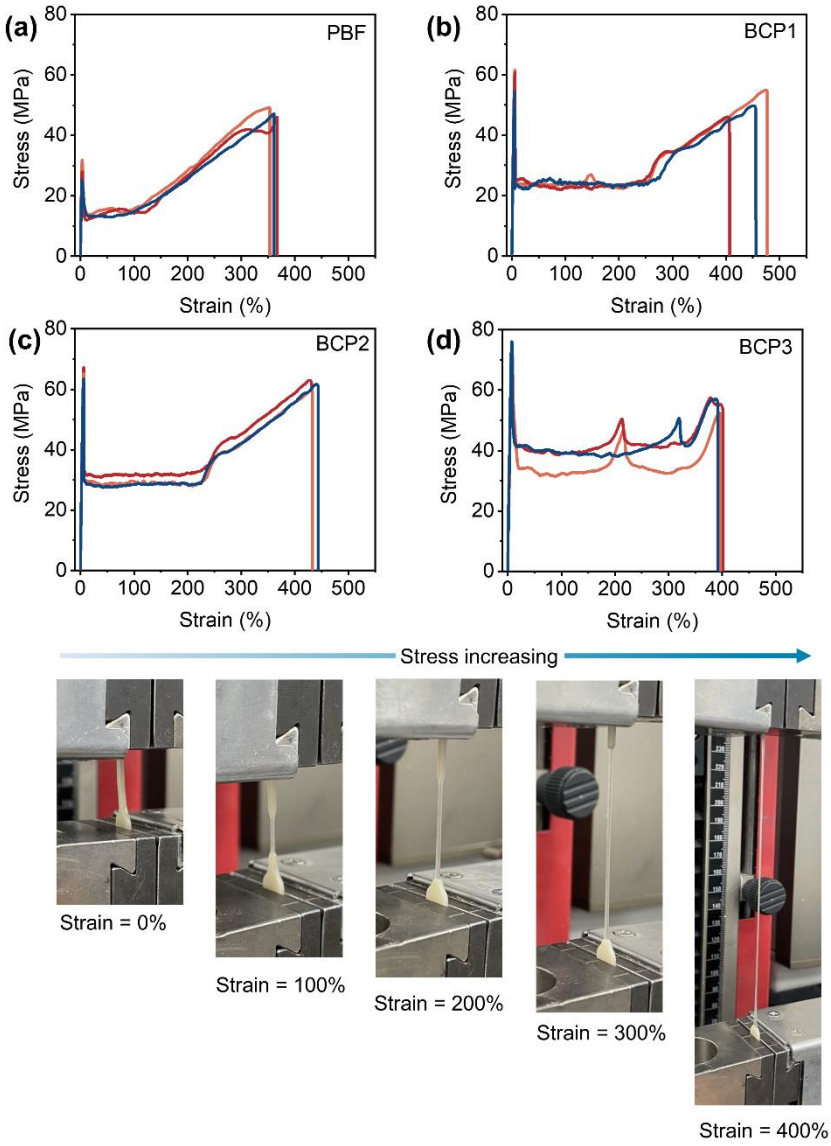

Figure S9. The stress-strain plots of PBF (a), BCP1 (b), BCP2 (c), and BCP3 (d) films. These BCP films exhibit largely enhanced mechanical properties, and the strengths and modulus of composites increased with the increasing of fillers. The digital photos of stress process for the BCP3 sample (e).

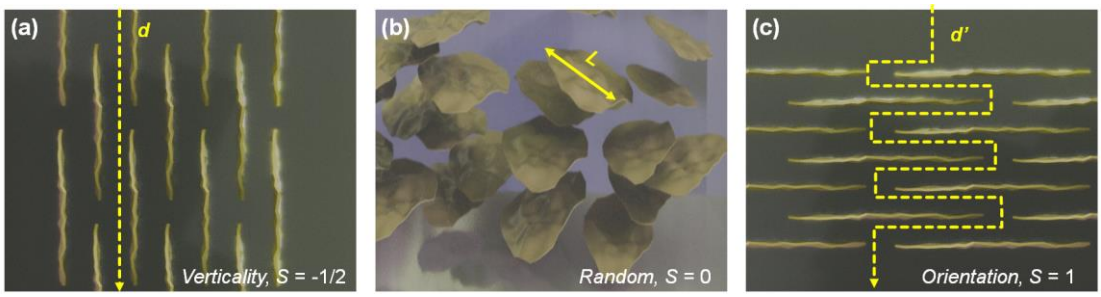

Figure S10. Schematic diagrams of the physical barrier mechanisms of MSSs composites. Tortuosity (τ) of the gas diffusion in the films was determined by *Nielsen* theory. The τ is defined as the ratio of the factual distance *d*' to the shortest distance *d*. The gas cannot penetrate into the sheets, while they must bypass the MSSs, causing tortuous pathways. As a result, the degree of tortuosity is related to aspect ratio L/W (L and W represent the lateral size and thickness of MSSs, respectively), orientation *S*, and content φ of the fillers, which can be approximately given by following [3].

$$\tau = \frac{d'}{d} = 1 + \frac{L}{2W} \times \varphi \times \frac{2}{3}\left(S + \frac{1}{2}\right) \qquad (S1)$$

where the orientation degree S can be defined by equation

$$S = \frac{1}{2}(3cos^2\theta - 1) \qquad (S2)$$

where when the sheets are verticality distribution, θ = 90° (*S* = -1/2); when the sheets are parallel arrangement, θ = 0° (*S* = 1), while the sheets are random distribution, θ = 54.74° (*S* = 0). The corresponding results can be found in Table S5.

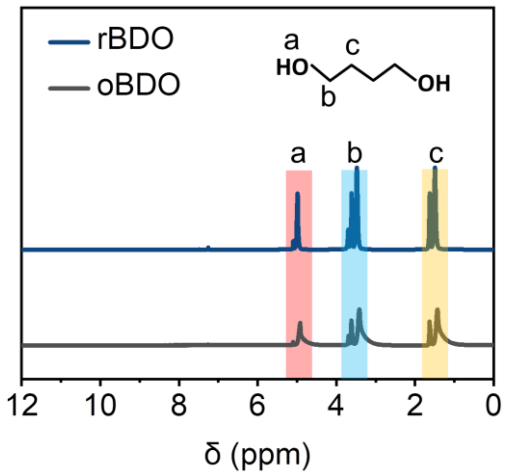

Figure S11. ^{1}H NMR spectra of standard BDO (oBDO) and recycled BDO (rBDO). Result demonstrates that rBDO shows the same ^{1}H NHR spectrum with the oBDO.

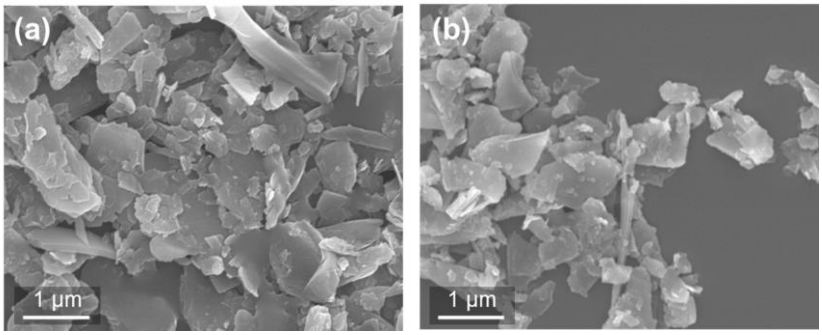

Figure S12. SEM image of the recycled MSSs (rMSSs). Results demonstrate that the rMSSs remained their original sheet-like structure during the chemical recycled process.

Table S1. Molecular weight and intrinsic viscosity [η_{sp}] of polyesters.

Sample	MSSs (wt%)	[ŋ]	M_n (g/mol)	M_w (g/mol)	PD
PBF	0.0	0.94	4.0×10^4	6.9×10^4	1.7
BCP1	0.1	0.97	3.7×10^4	7.0×10^4	1.9
BCP2	0.2	0.97	3.9×10^4	6.9×10^4	1.8
BCP3	0.3	1.05	4.1×10^4	7.8×10^4	1.9

Table S2. Mechanical properties parameters of different polyester materials.

Sample	σ_y[a] (MPa)	E[a] (GPa)	ε[a] (%)	τ[a] (MJ/m^3)
PBF	47 ± 2	1.4 ± 0.05	360 ± 7	96 ± 2
BCP1	58 ± 4	1.5 ± 0.1	445 ± 20	137 ± 18
BCP2	65 ± 2	1.5 ± 0.1	436 ± 7	166 ± 5
BCP3	76 ± 1	1.5 ± 0.1	397 ± 4	161 ± 18

[a]σ, E, ε, and τ refer to tensile strength, Young's modulus, elongation at break, and toughness, respectively.

Table S3. Mechanical properties of BCP and previously reported FDCA-based polyesters materials.

No.	Sample	σ_y (MPa)	σ_b (MPa)	ε (%)	Ref.
1	PEF	-	82	4	[4]
2	Mica/PEF	67	-	4.7	[5]
3	$PE_{91}Pe_9F$	80	-	29	[4]
4	$PE_{82}Pe_{18}F$	83	-	115	[4]
5	$PE_{66}Pe_{34}F$	75	-	181	[4]
6	$PE_{53}Pe_{47}F$	72	-	265	[4]
7	$PE_{37}Pe_{63}F$	49	-	185	[4]
8	$PE_{16}Pe_{84}F$	33	-	286	[4]
9	$PE_4Pe_{96}F$	-	20	315	[4]
10	$PE_{81}H_{19}F$	-	66	3	[6]
11	$PE_{72}H_{28}F$	71	-	54	[6]
12	$PE_{64}H_{36}F$	65	-	159	[6]
13	$PE_{48}H_{52}F$	48	-	275	[6]
14	$PE_{34}H_{66}F$	-	34	315	[6]
15	$PE_{12}H_{88}F$	-	38	148	[6]
16	PPF	-	29	3	[7]
17	PBF	-	21	157	[7]
18	PHF	-	42	22	[7]
19	PPeF	-	9	1050	[8]
20	**BCP**	**76**	-	**397**	**This work**

σ_y, σ_b, and ε refer to yield strength, break strength and elongation at break.

Table S4. Structural parameters of BCP at various strains calculated from 1D correlation function curves of the SAXS profile.

Sample	Strain (%)	L (nm) [a]	I_a (nm)[b]	I_c (nm)[c]	Φ[d]
BCP	0	10.7	7.1	3.6	0.33
	100	12	7.9	4.1	0.34
	200	11.2	7.4	3.9	0.34

[a]The long period length; [b]Amorphous thickness; [c] crystalline thickness; [b] linear crystallinity.

Table S5. Gas barrier properties of different polyester materials.

Sample	τ[a]	O_2[a]	BIFp	CO_2[a]	BIFp	H_2O[b]	BIFp
PBF	1.0	0.060	1.0	0.073	1.0	4.70	1.0
BCP1	1.4	0.0317	1.9	0.0435	1.7	2.15	2.2
BCP2	1.8	0.0245	2.5	0.0312	2.3	1.74	2.7
BCP3	2.2	0.0183	3.3	0.0244	3.0	1.49	3.2
PET	/	0.077	/	0.11	/	4.80	/

[a]The test was carried out at 0.1001 MPa, at 23 ºC, 50% relative humidity. 1 barrer = 10^{-10} cm^3 $cm/cm^2 \cdot s \cdot cm$ Hg. [b]The test was carried out at 38 ºC, 90% relative humidity, 10^{-14} g cm/cm^2 s Pa.

Table S6. Gas permeability coefficients for BCP and other polyester materials

Sample	CO_2 （barrer）	BIFp	O_2 （barrer）	BIFp	H_2O (g/(m^2 d)	H_2O (g·cm/(cm^2 s Pa)	BIFp	Ref
PE	6.29	1.0	1.58	1.0	7.9	/	1.0	[9]
PP	3.82	1.6	2.75	0.6	2.2	/	3.6	[10]
PET	0.11	63.5	0.077	20.5	/	4.8×10^{-14}	1.8	[11]
PEF	0.04	161.2	0.02	105.3	/	1.64×10^{-14}	4.9	[12]
$P_{14}BTF$	0.09	68.3	0.05	30.3	/	2.05×10^{-14}	3.9	[13]
$PBCF_{40}$	0.7	9.0	0.1	15.8	/	1.3×10^{-14}	0.1	[14]
$PBFGA_{20}$	0.05	125.8	0.02	75.2	/	2.65×10^{-14}	3.0	[15]
PBF	0.073	86.2	0.06	26.3	/	4.7×10^{-14}	1.8	This work
BCP	**0.024**	**262.1**	**0.018**	**87.8**	**/**	**1.48×10^{-14}**	**5.4**	**This work**

Table S7. Mechanical properties of physically recycled BCP.

Sample	σ (MPa)	*E* (GPa)	ε (%)	τ (MJ/m^3)
Original	76 ± 1	1.5 ± 0.1	397 ± 4	161 ± 18
1st	76 ± 1	1.5 ± 0.1	382 ± 5	159 ± 15
3th	73 ± 1	1.3 ± 0.1	409 ± 5	168 ± 16

Table S8. Mechanical properties of chemically recycled BCP.

Sample	σ (MPa)	*E* (GPa)	ε (%)	τ (MJ/m^3)
o-BCP	76 ± 1	1.5 ± 0.1	397 ± 4	161 ± 18
r-BCP	77± 1	1.5 ± 0.1	378 ± 5	159 ± 15

REFERENCE.

[1] Y. Gao, J. Zhang, H. Xu, X. Zhao, L. Zheng, X. Li, L. Yu, Structural Studies of 1-Butyl-3-methylimidazolium Tetrafluoroborate/TX-100/ p-Xylene Ionic Liquid Microemulsions, *ChemPhysChem* **2006**, 7, 1554-1561.

[2] D.G. Papageorgiou, N. Guigo, V. Tsanaktsis, S. Exarhopoulos, D.N. Bikiaris, N. Sbirrazzuoli, G.Z. Papageorgiou, Fast Crystallization and Melting Behavior of a Long-Spaced Aliphatic Furandicarboxylate Biobased Polyester, Poly(dodecylene 2,5-furanoate), *Ind. Eng. Chem. Res.* **2016**, 55, 5315-5326.

[3] J. Ding, H. Zhao, S. Shi, J. Su, Q. Chu, H. Wang, B. Fang, M.R. Miah, J. Wang, J. Zhu, High-Strength, High-Barrier Bio-Based Polyester Nanocomposite Films by Binary Multiscale Boron Nitride Nanosheets, *Adv. Funct. Mater.* **2024**, 34, 2308631.

[4] H. Xie, L. Wu, B.-G. Li, P. Dubois, Modification of Poly(ethylene 2,5-furandicarboxylate) with Biobased 1,5-Pentanediol: Significantly Toughened Copolyesters Retaining High Tensile Strength and O2 Barrier Property, *Biomacromolecules* **2019**, 20, 353-364.

[5] J. Ding, H. Wang, H. Zhao, S. Shi, J. Su, Q. Chu, B. Fang, M.R. Miah, J. Wang, J. Zhu, Large-Size ultrathin mica nanosheets: Reinforcements of biobased PEF polyester, *Giant* **2024**, 18, 100264.

[6] H. Xie, L. Wu, B.-G. Li, P. Dubois, Biobased Poly(ethylene-co-hexamethylene 2,5-furandicarboxylate) (PEHF) Copolyesters with Superior Tensile Properties, *Ind. Eng. Chem. Res.* **2018**, 57, 13094-13102.

[7] G. Guidotti, M. Soccio, M.C. García-Gutiérrez, T. Ezquerra, V. Siracusa, E. Gutiérrez-Fernández, A. Munari, N. Lotti, Fully Biobased Superpolymers of 2,5-Furandicarboxylic Acid with Different Functional Properties: From Rigid to Flexible, High Performant Packaging Materials, *ACS Sustainable Chem. Eng.* **2020**, 8, 9558-9568.

[8] X. Qu, G. Zhou, R. Wang, H. Zhang, Z. Wang, M. Jiang, J. Tang, Insights into high molecular weight poly(ethylene 2,5-furandicarboxylate) with satisfactory appearance: Roles of in-situ catalysis of metal zinc, *J. Ind. Eng. Chem.* **2021**, 99, 422-430.

[9] E. Jacquelot, E. Espuche, J.F. Gérard, J. Duchet, P. Mazabraud, Morphology and gas barrier properties of polyethylene-based nanocomposites, *J. Polym. Sci., Part B: Polym. Phys.* **2006**, 44, 431-440.

[10] M. Nuruddin, D.M. Korani, H. Jo, R.A. Chowdhury, F.J. Montes, J.A. Howarter, J.P. Youngblood, Gas and Water Vapor Barrier Performance of Cellulose Nanocrystal–Citric Acid-Coated Polypropylene for Flexible Packaging, *ACS Appl. Polym. Mater.* **2020**, 2, 4405-4414.

[11] L. Marangoni Júnior, R.M.V. Alves, C.Q. Moreira, M. Cristianini, M. Padula, C.A.R. Anjos, High-pressure processing effects on the barrier properties of flexible packaging materials, *J. Food Process. Preserv.* **2020**, 44, e14865.

[12] J. Yi, Y. Li, Y. Zhao, Z. Xu, Y. Wu, M. Jiang, G. Zhou, Development of a series of biobased poly(ethylene 2,5-furandicarboxylate-co-(5,5′-((phenethylazanediyl)-bis(methylene))bis(furan-5,2-diyl))dimethylene 2,5-furandicarboxylate) copolymers via a sustainable and mild route: promising “breathing” food packaging materials, *Green Chem.* **2022**, 24, 5181-5190.

[13] S. Tian, Y. Du, P. Wang, T. Chen, J. Xu, H. Yu, B. Guo, Effects of Different Isomers of Thiophenedicarboxylic Acids on the Synthesis and Properties of Thiophene-Based Sustainable Polyesters, *ACS Sustainable Chem. Eng.* **2023**, 11, 6652-6664.

[14] H. Hu, R. Zhang, J. Wang, W.B. Ying, J. Zhu, Synthesis and Structure-Property Relationship of Biobased Biodegradable Poly(butylene carbonate-co-furan-dicarboxylate), *ACS Sustainable Chem. Eng.* **2018**, 6, 7488-7498.

[15] H. Hu, R. Zhang, J. Wang, W.B. Ying, L. Shi, C. Yao, Z. Kong, K. Wang, J. Zhu,

A mild method to prepare high molecular weight poly(butylene furan-dicarboxylate-co-glycolate) copolyesters: effects of the glycolate content on thermal, mechanical, and barrier properties and biodegradability, *Green Chem.* **2019**, 21, 3013-3022.